

Thickness dependence, *in situ* measurements, and morphology of thermally controlled interdiffusion in polymer-C₆₀ photovoltaic devices

M. Drees,^{1,*} R. M. Davis,² and J. R. Hefflin^{1,†}¹*Department of Physics, Virginia Tech, Blacksburg, Virginia 24061, USA*²*Department of Chemical Engineering, Virginia Tech, Blacksburg, Virginia 24061, USA*

(Received 19 November 2003; revised manuscript received 20 February 2004; published 28 April 2004)

A series of detailed studies is presented in which heat-induced interdiffusion is used to create a gradient bulk-heterojunction of 2-methoxy-5-(2'-ethylhexyloxy)-1,4-phenylenevinylene (MEH-PPV) copolymer and C₆₀. Starting from a bilayer of spin-cast MEH-PPV and sublimed C₆₀, films are heated in the vicinity of the glass transition temperature of the polymer to induce an interdiffusion of polymer and fullerene. Variation of the polymer layer thickness shows that the photocurrents increase with decreasing layer thickness within the examined thickness regime as transport of the separated charges out of the film is improved. The interdiffusion was observed *in situ* by monitoring the photocurrents during the heating process and exhibited a rapid rise during the first five minutes. Cross-sectional transmission electron microscopy studies show that C₆₀ forms clusters of up to 30 nm in diameter in the polymer bulk of the interdiffused devices. This clustering of the fullerene molecules puts a significant constraint on the interdiffusion process that can be alleviated by use of donor-acceptor combinations with better miscibility.

DOI: 10.1103/PhysRevB.69.165320

PACS number(s): 73.50.Pz, 78.66.Qn, 82.35.Np

I. INTRODUCTION

The discovery of ultrafast photoinduced charge transfer from conducting polymers to the Buckminsterfullerene C₆₀ (Ref. 1) has fueled research towards organic photovoltaic devices.^{2–5} Upon photoexcitation of an electron-hole pair, the transfer of electrons from the polymer onto the fullerene leads to an efficient separation of charges that prevents luminescent recombination and is required in photovoltaic devices. Since the charge transfer can only occur if the photoexcitation on the polymer is within less than 10 nm of a C₆₀ molecule,^{6–8} close proximity of polymer and fullerene is essential for efficient charge separation. One approach for achieving such close proximity of the electron donor and acceptor materials is by creating a bulk heterojunction. This means that the donor and acceptor form an interface throughout the bulk of the active layer of the photovoltaic device. In this manner, photons absorbed anywhere within the active layer yield separated charges. However, a bulk-heterojunction formed by a blend of the donor and acceptor is not the ideal composition from the point of charge transport, which is improved by having a film that is donor-rich in the vicinity of the anode and acceptor-rich in the vicinity of the cathode.

We have recently reported an approach to create such a bulk heterojunction with a concentration gradient of donor and acceptor material by using thermally controlled interdiffusion of polymer and fullerene layers.⁹ Photoluminescence quenching with concomitant increase in photocurrent in interdiffused devices showed the improved interface between polymer and fullerene throughout the bulk of the active layer. Here, we present additional studies of interdiffused polymer/fullerene layers that provide further characterization of the interdiffusion process and the morphology of the resulting polymer/fullerene film. Variation of the polymer layer thickness shows that, within the examined thickness regime

(70–110 nm), the photocurrents in the interdiffused devices increase with decreasing thickness as a result of improved charge transport out of the film. Transmission electron microscopy (TEM) studies on cross sections of the films reveal that C₆₀ forms clusters of up to 30 nm diameter in the polymer bulk of the interdiffused devices. These large clusters are a constraint for the interdiffusion in this pair of relatively immiscible materials and therefore hinder the creation of a bulk heterojunction. In addition, the interdiffusion was observed *in situ* by monitoring the photocurrents during the heat treatment.

II. EXPERIMENTAL

Photovoltaic devices were prepared by first spin-coating a poly(3,4-ethylenedioxythiophene):poly(styrenesulfonate) complex (PEDOT:PSS) (Bayer Corp.) onto indium tin oxide (ITO)-covered glass substrates. Subsequently, 2-methoxy-5-(2'-ethylhexyloxy)-1,4-phenylenevinylene (MEH-PPV) copolymer (M.W. ~85,000, H.W. Sands Corp.) was spin-coated from a 1% wt/vol chlorobenzene solution. By varying the spin speed between 2000 and 4000 rpm, film thicknesses of 110, 90, and 70 nm were achieved. After annealing films under vacuum at 150 °C to remove water and solvents, a 100 nm C₆₀ (MER Corp.) film was sublimed onto the MEH-PPV. This polymer/fullerene bilayer structure was then heated in a nitrogen glove box at 150 or 250 °C for 5 min to induce an interdiffusion of the two layers. Finally, a 200 nm thick Al layer was evaporated under vacuum as the cathode.

Film thicknesses were determined using the optical density values obtained with a Filmetrics F20-UV thin film spectrometer system from transmission and reflection data. The absorption coefficients used for calibration are $18 \times 10^4 \text{ cm}^{-1}$ at 490 nm for MEH-PPV and $6 \times 10^4 \text{ cm}^{-1}$ at 435 nm for C₆₀ as determined by interference fringes in the reflection spectra of thicker films.

The photoresponsivity spectra were recorded under argon

atmosphere by illuminating the samples through the glass and ITO with light from a 300 W Xe lamp that was passed through a CVI CM100 monochromator to select wavelengths between 300 and 700 nm and recording the photocurrents with a Keithley 485 picoammeter. To normalize the power spectrum of the Xe-lamp/monochromator system, a calibrated Si photodiode was used in the same setup.

For the *in situ* studies, complete devices (including Al cathode) were first prepared without the interdiffusion heating step. This way, the devices could be measured in the unheated bilayer structure before the heat treatment. Devices were then heated in an argon atmosphere while monitoring the photocurrents in the same setup used for photoresponsivity measurements.

To study the morphology of the interdiffused devices, transmission electron microscopy was performed on cross sections of the films. MEH-PPV/C₆₀ bilayers were prepared on glass substrates and taken through the interdiffusion heating step. The films were then lifted off the substrate by submerging them in deionized water. After drying films overnight in a nitrogen glovebox, films were imbedded in an epoxy and slices of 50 nm thickness revealing the cross section of the films were microtomed with a Reichert-Jung Ultracut E microtome. These specimens were studied in a Philips 420T TEM system at 100 keV.

III. THICKNESS VARIATION OF THE POLYMER LAYER

While the fraction of incident photons absorbed increases with the thickness of the MEH-PPV, the ability to extract separated charges decreases due to the relatively low electrical conductivity. To examine these competing effects, MEH-PPV/C₆₀ bilayer devices with 70, 90, and 110 nm polymer and 100 nm fullerene layer thicknesses were prepared without heating and with interdiffusion at 250 and 150 °C. The photoresponsivity spectra of the unheated bilayer devices are shown in Fig. 1. With decreasing polymer layer thickness, the photoresponsivity of the devices increases throughout most of the spectrum. The increase in the photocurrents is due to two reasons: (1) the number of photons that can reach the polymer-fullerene interface where efficient charge separation occurs is increased in devices with thinner polymer films and (2) the distance that charges have to travel to the collecting electrodes is reduced, therefore reducing the series resistance of the device. In addition to the increase in photocurrent, the peak position of the photocurrents shifts towards the absorption maximum at 490 nm (see the inset of Fig. 1 for absorption spectrum). The peak photocurrent moves from $\lambda = 575$ nm in the 110 nm device to $\lambda = 560$ nm and $\lambda = 540$ nm in the 90 and 70 nm devices, respectively. This behavior can be explained by a reduction in the filter effect^{10,11} of the MEH-PPV bulk with decreasing layer thickness. Since the MEH-PPV layer acts like an optical filter, most of the photons in wavelength regions of strong absorption are absorbed near the anode/MEH-PPV interface and do not reach the MEH-PPV/C₆₀ interface where efficient charge separation occurs. Therefore, devices with a filter effect exhibit low photocurrents in regions of strong absorption which leads to a mismatch between the absorption spectrum

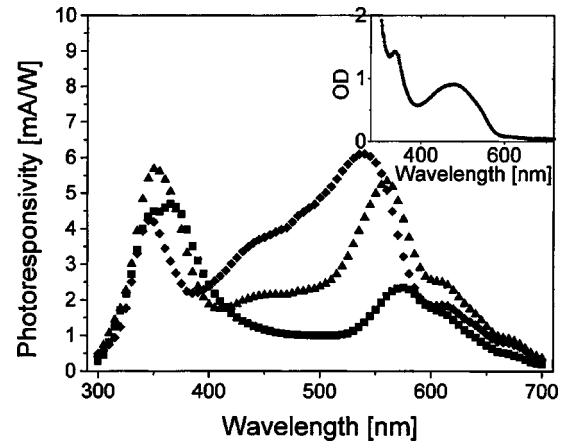


FIG. 1. Photoresponsivity of unheated MEH-PPV/C₆₀ bilayer devices with varying MEH-PPV thickness. The photocurrents increase with decreasing MEH-PPV thickness. In addition, the photocurrent peak at $\lambda = 575$ nm for 110 nm MEH-PPV (squares) shifts to 560 and 540 nm for 90 nm MEH-PPV (triangles) and 70 nm MEH-PPV (diamonds), respectively. The C₆₀ film thickness was 100 nm for all devices. The inset shows the optical density of a MEH-PPV/C₆₀ bilayer device with 90/100 nm layer thickness, respectively.

and photocurrent spectrum. Since the filter effect is reduced with decreasing MEH-PPV layer thickness, the peak of the photocurrent spectrum shifts towards the absorption peak. This mismatch between absorption and photocurrent spectra can thus be used to characterize the quality of the bulk-heterojunction in the active layer of the device. Only devices with a bulk heterojunction will have similar absorption and photocurrent spectra.

Next, we prepared devices with the same set of polymer and fullerene layer thicknesses that were heated at 150 °C for 5 min, which is below the glass transition temperature of MEH-PPV (the T_g of MEH-PPV was confirmed to be ~ 230 °C by differential scanning calorimetry analysis). The photoresponsivity spectra (Fig. 2) again show the same trend of increasing photocurrents with decreasing polymer layer

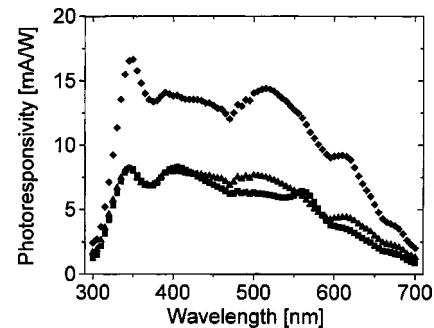


FIG. 2. Photoresponsivity of MEH-PPV/C₆₀ bilayer devices heated at 150 °C with varying MEH-PPV thickness. A decrease in MEH-PPV thickness results in an increase of photocurrents. In all devices, the filter effect is reduced because of interdiffusion. Devices shown have MEH-PPV thickness of 110 nm (squares), 90 nm (triangles), and 70 nm (diamonds). C₆₀ thickness is 100 nm for all devices.

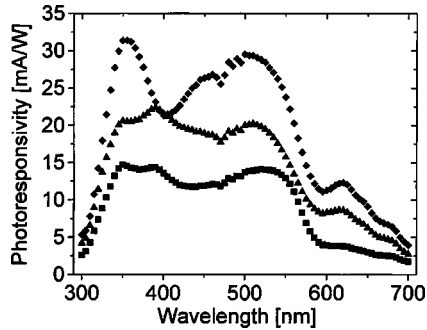


FIG. 3. Photoresponsivity of MEH-PPV/C₆₀ bilayer devices heated at 250 °C with varying MEH-PPV thickness. A decrease in MEH-PPV thickness results in an increase of photocurrents. Devices shown have MEH-PPV thickness of 110 nm (squares), 90 nm (triangles), and 70 nm (diamonds). C₆₀ thickness is 100 nm for all devices. The photocurrent spectrum of the 70 nm device is very similar in shape to the absorption spectrum which indicates that the interdiffusion resulted in a bulk heterojunction device.

thickness. In addition, the shape of the photoresponsivity has changed dramatically due to the heat-treatment. The low photocurrents in regions of strong absorption caused by the filter effect are no longer observed. On the other hand, the peak photocurrents do not increase dramatically compared to the unheated bilayer devices. This shows that through heating the devices below the polymer T_g , C₆₀ can partially diffuse into the polymer layer. The amount of C₆₀ is enough to reduce the filter effect of the devices by providing charge transfer sites but not enough to create substantial continuous conducting paths for the separated charges to be efficiently transported out of the device.

Figure 3 shows the photoresponsivity for a similar set of devices heated above the MEH-PPV T_g at 250 °C for 5 min. The interdiffusion leads to an order of magnitude increase in the photocurrents throughout most of the spectrum. Again, devices with thinner polymer layers show higher photocurrents. Importantly, the shape of the photocurrent spectrum for devices with 70 nm MEH-PPV finally starts to match the absorption spectrum of the devices, indicative that a bulk heterojunction has been achieved.

I-V curves for the devices with various MEH-PPV thicknesses are similar to those reported in Ref. 9. The *I-V* characteristics, fill factors, and monochromatic power conversion efficiencies of the various devices are listed in Table I. While the open circuit voltage and the short circuit current are improved by the interdiffusion, the fill factor is reduced. The overall efficiency of our unheated bilayer devices is comparable to efficiencies previously observed in MEH-PPV/C₆₀ bilayers.¹⁰ The 0.3% (under monochromatic illumination) efficiency of the device with 70 nm MEH-PPV heated at 250 °C is low compared to MEH-PPV-fullerene blend devices, which have obtained 2.9% monochromatic efficiency.¹² But these latter devices utilize a highly soluble C₆₀ derivative that is known to provide enhanced efficiency.

These results indicate that the interdiffusion of MEH-PPV and C₆₀ is most likely restricted by the strong phase separation of polymer and fullerene in this pair of materials. The C₆₀ does not easily diffuse long distances into the MEH-PPV. Therefore, the charge transfer is not optimized throughout the entire bulk and only the interdiffused devices with 70 nm of MEH-PPV come close to forming a bulk heterojunction, which is indicated by a better match of photoresponsivity and absorption spectrum. The overall efficiency of the devices is low because of the difficulty of the interdiffusion process with this pair of materials.

It should also be noted here that in devices with even thinner polymer layers the photocurrents are expected to eventually decrease. Even though the series resistance is continually reduced, the percentage of absorbed photons is concomitantly reduced and this effect at some point outweighs the reduction in series resistance.

IV. *IN SITU* OBSERVATION OF THE INTERDIFFUSION

In situ studies of the interdiffusion during the heating process were carried out to determine the optimum conditions for the time-temperature thermal profile. In the studies presented above, the interdiffusion heating was done before the final production step of depositing the top electrode. Because of this, measurement of the photoresponse of the same device before and after the heat treatment was not possible.

TABLE I. *I-V* characteristics, fill factor, and monochromatic power conversion efficiency for MEH-PPV/C₆₀ devices with varying thicknesses and thermal treatment under monochromatic illumination (470 nm, 3.8 mW/cm²).

MEH-PPV thickness (nm)	Interdiffusion temperature	V_{OC} [V]	I_{SC} [mA/cm ²]	FF	Efficiency [%]
110	unheated	0.3	3.8×10^{-3}	0.5	0.02
90	unheated	0.4	7.9×10^{-3}	0.4	0.03
70	unheated	0.4	16×10^{-3}	0.39	0.07
110	150 °C	0.6	24×10^{-3}	0.25	0.10
90	150 °C	0.6	26×10^{-3}	0.24	0.10
70	150 °C	0.6	28×10^{-3}	0.25	0.11
110	250 °C	0.5	42×10^{-3}	0.25	0.14
90	250 °C	0.5	67×10^{-3}	0.29	0.26
70	250 °C	0.5	92×10^{-3}	0.25	0.30

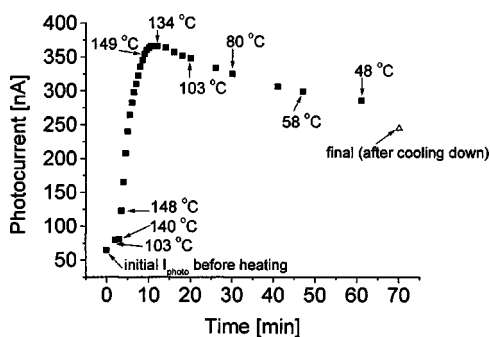


FIG. 4. *In situ* photocurrent measurements. The photocurrent of a 70 nm MEH-PPV/110 nm C_{60} device was observed during the interdiffusion heating at 150 °C (470 nm, 3.8 mW/cm² illumination). The squares show the photocurrent during the thermal treatment. The temperature at various times is indicated. The final photocurrent of the device (after complete cooling down to room temperature) is given by the open triangle.

This was initially done to prevent damage of the devices due to cracking of the polymer bulk that was often observed when heating was carried out in thick (layer thicknesses of 120 nm or more) polymer films. We found, however, that this problem was alleviated with thinner films at 150 °C, thus enabling *in situ* observations.

Figure 4 shows the photocurrent of an MEH-PPV/ C_{60} bilayer with 70 nm of MEH-PPV and 110 nm of C_{60} that was monitored during the heating. The data shown are the raw photocurrent values resulting from illumination of the device with monochromatic light (470 nm, 3.8 mW/cm²). The temperature of the hot stage is indicated for selected times.

With increasing temperature, the photocurrent of the illuminated sample rapidly begins to rise. When the temperature reaches 150 °C, it is maintained for 5 min before the hot plate is turned off and the temperature starts decreasing. While the temperature stays constant at 150 °C, the photocurrent continually increases and even after the temperature starts decreasing, it rises further for a few minutes. The photocurrent then levels off and finally starts decreasing. The final photocurrent after cooling to room temperature is four times larger than the initial photocurrent. Since the photocurrent decreases to some extent during cooling, it is clear that not all of the increase in photocurrent during the heating is due to interdiffusion. Part of it is simply due to the elevated temperature. Since charge transport in conjugated polymers and C_{60} is typically a hopping process, which is thermally activated, the photocurrents are expected to be larger at higher temperatures because of the increased conductivity. This temperature dependence of the short circuit current has been previously observed in polymer-fullerene photovoltaic devices.^{13,14}

The change in the photoresponsivity spectrum due to the *in situ* heat treatment is shown in Fig. 5. To better see the change in the shape, the data were normalized to the peak at 555 nm (while the spectrum obtained before heating was divided by 2.9, the spectrum after heating was divided by 6.8). The photocurrent spectrum after heating clearly shows a reduction in the filter effect. However, compared to devices that were heated without the Al electrode, the reduction in

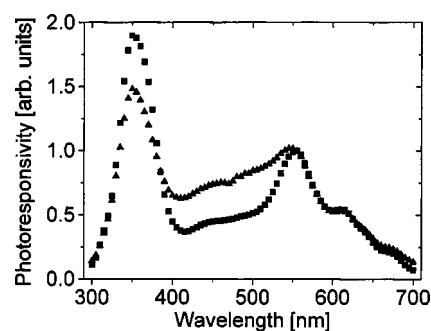


FIG. 5. Normalized photoresponsivity spectra of an MEH-PPV/ C_{60} bilayer device before and after heat treatment. The photoresponsivity spectra were normalized to the peak at 555 nm to show the difference in shape before (squares) and after (triangles) interdiffusion. The filter effect is clearly reduced by the interdiffusion.

the filter effect is not as strong as that observed when the devices were heated without the Al electrode. This is believed to be due to constraint that the Al electrode places on the interdiffusion of C_{60} into the MEH-PPV bulk.

The interdiffusion could not be observed *in situ* at temperatures above T_g of MEH-PPV. Typically, the photocurrent signal decreased to zero at temperatures in the vicinity of T_g and did not recover even after cooling of the device. The reason for this permanent device failure could not be determined but is possibly due to delamination of the electrode from the organic film. It is apparent, though, that device failure is in the vicinity of the glass transition temperature of the polymer where the polymer chains can undergo segmental motion.

It should be mentioned here that heating the devices for more than 5 min at 150 °C led to a decrease in photocurrent at the elevated temperature. The time after which this decrease started varied between devices from 5 to 10 min after reaching 150 °C.

V. MORPHOLOGY OF THE INTERDIFFUSED DEVICES

The TEM image of the cross section of an unheated MEH-PPV/ C_{60} bilayer is shown in Fig. 6. By imaging the cross section of an MEH-PPV single layer, it was determined that the light phase is the polymer. The dark phase is therefore C_{60} . The gray background surrounding the film is due to the epoxy in which the film is imbedded. The image shows a smooth, distinct interface between polymer and fullerene, which is expected from an unheated bilayer. A very similar image was obtained for bilayers heated at 150 °C. Since the TEM image does not provide atomic resolution, it does not provide information concerning single C_{60} molecules or very small clusters of C_{60} diffused into the MEH-PPV. The reduction of the filter effect in the devices heated at 150 °C indicates that some interdiffusion occurs, but the TEM image shows that no large-scale intermixing of the two materials takes place.

The TEM image (Fig. 7) of a device heated at 250 °C (above T_g of MEH-PPV) shows dramatic changes compared to the unheated bilayer. The distinct smooth interface be-



FIG. 6. TEM image of an unheated MEH-PPV/ C_{60} bilayer. The light phase is MEH-PPV, the dark phase is C_{60} , and the gray background is from the epoxy. The picture shows a distinct and smooth interface between the two materials.

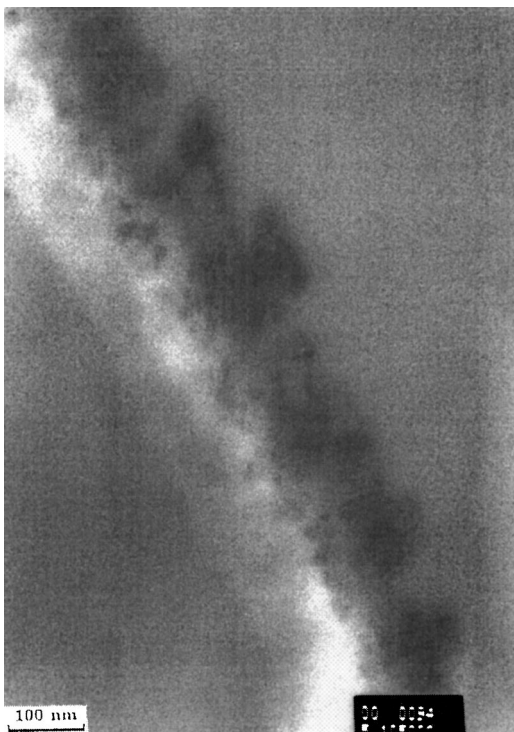


FIG. 7. TEM image of an MEH-PPV/ C_{60} bilayer heated at 250 °C for 5 min. The image shows a rough interface with clusters of C_{60} with a diameter of up to 30 nm present in the MEH-PPV bulk.

tween the two materials has vanished. Instead, clusters of C_{60} with diameters up to 30 nm have migrated into the MEH-PPV bulk. The image clearly shows that there is not a continuous concentration gradient of donor and acceptor materials from one end of the film to the other. Instead, there is a polymer-rich phase at one end and a fullerene-rich phase at the other end of the cross section with a blend of large C_{60} clusters and MEH-PPV in the middle. The formation of C_{60} clusters is partly due to the strong tendency towards crystallization of C_{60} (Ref. 15) and due to the tendency of MEH-PPV and C_{60} to phase separate. It is therefore not surprising that the interdiffusion is limited in these materials. In fact, in light of the TEM images, it is remarkable that thermally induced interdiffusion is so effective in enhancing the photovoltaic performance of this material system. It might be expected that a more miscible material pair would yield further improvement. This has indeed been confirmed and will be reported in a separate publication.

The results of the TEM studies help explain the polymer thickness dependence of the devices. It was found that a good bulk heterojunction was only formed for thin polymer layers. Observing the size of C_{60} clusters in the polymer bulk and keeping in mind that the two materials tend to stay in separate phases, it is clear that the C_{60} will not diffuse long distances into the MEH-PPV bulk. This then limits the ability of the two materials to form a good blend with close proximity of polymer and fullerene and thus yields less than optimal charge separation in the bulk of the active layer.

VI. CONCLUSIONS

The photocurrent in polymer/fullerene photovoltaic devices has been examined as a function of the polymer layer thickness. The studies were carried out on devices with and without the use of thermally induced interdiffusion of the layers to create a gradient bulk heterojunction. For MEH-PPV in combination with C_{60} , the interdiffusion process is limited due to strong phase separation between the polymer and fullerene. TEM studies show a tendency of C_{60} to form large clusters of up to 30 nm in diameter in the polymer bulk. These clusters illustrate the strong phase separation of MEH-PPV and C_{60} that limits the interdiffusion process and therefore formation of a bulk heterojunction. Therefore, our observation is that a bulk-heterojunction is only formed by interdiffusion in devices with thin MEH-PPV layers, in our case 70 nm.

In situ studies showed that the interdiffusion can be observed by monitoring the photocurrent of the device. An optimization of the time-temperature profile for the interdiffusion of the materials can therefore be easily implemented. The studies also showed that in the fully built devices the Al electrode places some additional constraint on the interdiffusion process.

These studies show that thermally induced interdiffusion is a suitable method to create polymer/fullerene bulk-heterojunction photovoltaic devices with a concentration gradient of polymer and fullerene from anode to cathode of the device. However, the choice of materials is a critical issue for effective interdiffusion. The polymer and fullerene need

to be well miscible for good mass transport to occur during the heating. Enhanced photovoltaic performance of devices utilizing a more miscible donor/acceptor pair will be reported separately.

ACKNOWLEDGMENTS

We would like to thank Steve McCartney at Virginia Tech for his help with the TEM studies.

*Present Address: Linz Institute for Organic Solar Cells (LIOS), Physical Chemistry, Johannes Kepler University Linz, Altenberger Str. 69, A-4040 Linz, Austria.

†Author to whom correspondence should be addressed.

¹N. S. Sariciftci, L. Smilowitz, A. J. Heeger, and F. Wudl, *Science* **258**, 1474 (1992).

²S. E. Shaheen, C. J. Brabec, N. S. Sariciftci, F. Padinger, T. Fromherz, and J. C. Hummelen, *Appl. Phys. Lett.* **78**, 841 (2001).

³M. Granstrom, K. Petritsch, A. C. Arias, A. Lux, M. R. Andersson, and R. H. Friend, *Nature (London)* **395**, 257 (1998).

⁴G. Yu, J. Gao, J. C. Hummelen, F. Wudl, and A. J. Heeger, *Science* **270**, 1789 (1995).

⁵L. Chen, D. Godovsky, O. Inganäs, J. C. Hummelen, R. A. J. Janssens, M. Svensson, and M. R. Andersson, *Adv. Mater. (Weinheim, Ger.)* **12**, 1367 (2000).

⁶D. Vacar, E. S. Maniloff, D. W. McBranch, and A. J. Heeger, *Phys. Rev. B* **56**, 4573 (1997).

⁷J. J. M. Halls, K. Pichler, R. H. Friend, S. C. Moratti, and A. B.

Holmes, *Appl. Phys. Lett.* **68**, 3120 (1996).

⁸A. Haugeneder, M. Neges, C. Kallinger, W. Spirkl, U. Lemmer, J. Feldmann, U. Scherf, E. Harth, A. Gügel, and K. Müllen, *Phys. Rev. B* **59**, 15346 (1999).

⁹M. Drees, K. Premaratne, W. Graupner, J. R. Hefflin, R. M. Davis, D. Marciu, and M. Miller, *Appl. Phys. Lett.* **81**, 4607 (2002).

¹⁰N. S. Sariciftci, L. Smilowitz, A. J. Heeger, and F. Wudl, *Synth. Met.* **59**, 333 (1993).

¹¹A. C. Arias, M. Granstrom, D. S. Thomas, K. Petrisch, and R. H. Friend, *Phys. Rev. B* **60**, 1854 (1999).

¹²G. Yu, J. Gao, J. C. Hummelen, F. Wudl, and A. J. Heeger, *Science* **270**, 1789 (1995).

¹³E. A. Katz, D. Faiman, S. M. Tuladhar, J. M. Kroon, M. M. Wienk, T. Fromherz, F. Padinger, C. J. Brabec, and N. S. Sariciftci, *J. Appl. Phys.* **90**, 5343 (2001).

¹⁴I. Riedel, J. Parisi, V. Dyakonov, L. Lutsen, D. Vanderzande, and J. C. Hummelen, *Adv. Funct. Mater.* **14**, 38 (2004).

¹⁵C. Y. Yang and A. J. Heeger, *Synth. Met.* **83**, 85 (1996).